Bursting-Layer Modeling Based on the Assumption of the Averaged Sea Surface for Strong Wind-Driven Currents

TOMOKAZU MURAKAMI

Department of Architecture and Civil Engineering, Toyohashi University of Technology, Aichi, Japan

TAKASHI YASUDA

Environmental and Renewable Energy Systems Division, Gifu University, Gifu, Japan

(Manuscript received 26 April 2006, in final form 2 July 2007)

ABSTRACT

In the sea, which is affected by strong winds that cover the water surface with wind-wave breakers, the sea surface layer, called the bursting layer by authors, is generated immediately below the mean water level. For treatment of strong wind-driven currents, it is necessary to model the bursting layer correctly based on observed data. However, an essential difficulty occurs in that, because of large water surface displacement caused by developed wind waves, water particle velocities above the wave trough level cannot be measured continuously in the Eulerian coordinates when measuring the velocity of strong wind-driven currents. Consequently, it is impossible to apply the Reynolds average rule to the velocity field above the wave trough level.

In this study, an experiment that uses a wind-wave tank with a double bottom is performed to measure the horizontal velocity of currents driven only by the wind stress. The vertical distribution up to the mean water level is determined to make its vertically integrated value agree with the total mass flux of the wind-driven currents. Furthermore, the vertical distribution of the Reynolds stress is derived by solving a Reynolds equation; its solution agrees with the given velocity distribution. Numerical simulation was performed to reproduce the strong wind-driven currents. Results showed that the bursting-layer model can correctly calculate the steep vertical distribution of the current velocity in the bursting layer.

1. Introduction

Coastal ocean currents driven by strong winds of typhoons and other storms accompany the developed wind-wave breakers. Such currents cause storm surge disasters, large-scale beach changes, environmental changes in inner bays, and other problems. Particularly, the vertical distributions are important because they strongly influence those problems. However, conventional models of wind-driven currents have merely evaluated the influence of the developed wind-wave breakers in a boundary condition and do not treat it directly as breaker stress, which is the Reynolds stress generated by the breaking waves, and governs the vertical distribution of the wind-driven current velocities. For that reason, in situations where the wind speed increases, conventional models can only slightly explain the experimental result presented by Ogasawara and Yasuda (2004): the mass transported within the strong wind-affected surface layer amounts to 20%–30% of the total mass flux of the wind-driven current. Therefore, investigation and subsequent modeling of the turbulent structure of the sea surface boundary layer that dominates the vertical distribution of strong wind-driven currents are required from the viewpoint of disaster prevention and coastal environment preservation.

Recent advancements in field observation technology enable us to obtain various measurement data that allow for clarification of sea surface boundary processes of wind-driven currents when the wind speed is not strong, but normal. Kitaigorodskii et al. (1983) carried out current velocity measurements using an oceanic buoy in Lake Ontario. That study subsequently pointed

---

Corresponding author address: Dr. Tomokazu Murakami, Department of Architecture and Civil Engineering, Toyohashi University of Technology, 1-1 Hibarigaoka, Tempakucho, Toyohashi, Aichi, Japan.
E-mail: murakami@jughead.tutrp.tut.ac.jp

DOI: 10.1175/2007JPO3618.1

out that a turbulent boundary layer exists immediately below the sea surface and that the energy dissipation rate in the layer is two orders or more greater than the rate given by the logarithmic law. Thorpe (1992) reported similar results based on the interpretation of acoustic reflections from bubbles generated by breaking waves. Moreover, Gargett (1989), from the measured vertical distribution of the horizontal current velocity, inferred a dissipation rate that decays faster than the first-power law of the depth below the sea surface. Those studies indicated that the sea surface turbulent boundary layer must be incorporated into the treatment of wind-driven currents.

However, the respective values of the wind speed and significant wave height in these field observations were, at most, 11 m s^{-1} and 0.58 m. Observation of currents driven by strong winds has not been performed, although such observations are necessary to produce a model of strong wind-driven currents. Perhaps such a study has been avoided because it presents a salient difficulty: the velocity data for the layer immediately below the sea surface cannot be obtained easily because the sea surface is covered with developed wind-wave breakers. Nevertheless, data that are indispensable to clarify the phenomena of sea surface boundary processes affected by strong winds are obtainable by performing wind-wave tank experiments, although a problem of the similarity law remains. Therefore, investigations of water particle velocity fields in the sea surface boundary layer can be greatly advanced by performing repeated measurements in strong wind conditions. Cheung and Street (1988b) developed a wave-following coordinate system in a wind-wave tank. They measured wind-affected water particle velocities in the zone between the mean water level (MWL) and the wave trough level (WTL) in an Eulerian coordinate system, but for the condition of low wind speeds of 1.7–6.1 m s^{-1}. Their results showed that the vertical distribution of the horizontal mean velocity below the water surface corresponded to a viscous sublayer (logarithmic law) in the Eulerian coordinate system. In addition, Banner and Peirson (1998) performed measurements of wind-affected velocity fields immediately below the water surface using a particle image velocimetry (PIV) technique and showed that characteristics of surface sublayer flow were influenced by microscale breaking events. Furthermore, Zhang and Cox (1999) measured the water particle velocity fields immediately below the water surface under the condition of earlier wind-wave measurements and found vortices immediately below the water surface. Moreover, their results showed that the surface boundary layer is intermittently either a viscous laminar flow or turbulent flow, depending on whether these vortices are free or attached to the surface; these vortices contribute greatly to small-scale mixing at the air–sea interface.

Therefore, studies to clarify the turbulent flow structures under wind waves have been performed using a wind-wave tank that facilitates repeated measurements and development of measuring instruments. However, some problems occur when experiments to examine currents driven by strong winds are performed using the wind-wave tank, even if the problem related to the similarity law is excluded. One obstacle was pointed out by Lin and Gad-el-Hak (1984): experiments using a conventional closed-end wind-wave tank suffer from return flow induced by the reverse pressure gradient, which is balanced with the wind stress together with the shear stress of the bottom and sidewalls. Because of the reverse pressure gradient, the experiments cannot give correct velocity information related to currents driven solely by wind stress. Another hurdle is that it is almost impossible to measure the velocity field immediately below a water surface affected by strong winds: such water surfaces are covered by developed wind waves accompanied by air bubbles caused by the breaking waves, airflow separation, and large water surface displacements. Of course, if the wind speeds are not so strong, then the aforementioned measuring instruments developed by Cheung and Street (1988b), Banner and Peirson (1998), and Zhang and Cox (1999), in which the maximum wind speed in these studies is at most 8.5 m s^{-1}, are suitable to obtain data of the velocity fields immediately below the water surface because influences of mixed air bubbles and intensive water surface elevations caused by developed wind waves are negligible. However, these influences are not negligible in the condition of strong winds, which are of interest here. Consequently, it is impossible to perform accurate measurements in the zone $|z|/H_s = 0$ to -0.2 (H_s is the significant wave height) immediately below the MWL, as pointed out by Soloviev and Lukas (2006), even if a wave-following coordinate system were used. Ogasawara and Yasuda (2004) grappled with these problems and solved the former problem by developing a wind-wave tank with a double bottom. It can measure the vertically averaged horizontal velocity of the wind-driven current caused solely by wind stress. Furthermore, they developed a high-resolution PIV system that can analyze rapidly moving and intensely fluctuating water particles affected by breaking waves. They obtained information of the vertical distribution up to the MWL of the horizontal mean velocity. Their results revealed that a turbulent boundary layer with strong turbulence is generated immediately below the MWL by the breaker action. Furthermore, the vertical gradient of velocity in the layer is very steep and obeys a power law. In addition, results clarified that the mass transported within the boundary layer amounts to about 20%–30% of the total mass flux of the wind-driven current, in spite of the fact that the layer is much thinner than the seawater depth and almost corresponds to the significant wave height. This fact suggests that surface layers affected by wind-wave breaking are important for coastal ocean currents driven by strong winds. Therefore, for the treatment of coastal ocean currents affected by strong winds, it is necessary to model the breaker stress generating the boundary layer correctly based on accurate measurement data.

In conventional models of wind-driven currents (Craig and Banner 1994; Mellor and Blumberg 2004), the influence of breaking waves is merely incorporated into a boundary condition at the averaged sea level of the Mellor–Yamada turbulence closure model. However, water particle velocities in the sea surface layer, affected by strong winds, are dominated by the vertically changing driving force caused by the breaker turbulence and disturbance associated with air bubbles and airflow separation. For those reasons, it is questionable how to evaluate their influence using only the boundary condition at the sea surface. Thais and Magnaudet (1995) and Magnaudet and Thais (1995) presented a technique to separate wind-affected velocity fields into linear and nonlinear orbital potential motion, orbital rotational motion, and turbulent motion; they analytically modeled the Reynolds stress caused according to these three motions. Craig (1996) also proposed a method to calculate the vertical distribution of the current velocity by giving the thickness of the wave-affected layer directly from the measured value in the water tank experiment by Cheung and Street (1988a) and derived the value of an eddy viscous coefficient from the turbulent kinetic energy obtained as a solution of the turbulent kinetic energy equation. However, the following problems remain in these models: The measurement values used are affected by the return flow, which causes the problem described above. An additional problem is that the vertical distribution of the horizontal velocity is not determined near the MWL. Because the horizontal velocity in the aforementioned model developed by Thais and Magnaudet (1995) and Magnaudet and Thais (1995) was calculated by combining a potential wave theory and the exact solution of the Gerstner wave, it is unable to incorporate the influence of mixed air bubbles and intensive water surface elevation caused by the developed wind waves. This is an important problem in the velocity measurement of strong wind-driven currents: it is impossible in an Eulerian coordinate system to measure water particle velocities continuously above the WTL because of the large displacement of the water surface resulting from developed wind waves. Therefore, because the domain between MWL and WTL becomes a void zone of measurements, it is also impossible to apply the Reynolds average rule to the turbulent flow components. In fact, direct measurement of the turbulent flow components required to calculate the Reynolds stress is impossible. For that reason, it is almost impossible to model the actual physical phenomena of the sea surface turbulent and aerated boundary layer (bursting layer) affected by strong winds using the microscopic modeling based on the measurement velocity data of the turbulent flow. Notwithstanding these great difficulties, because the bursting layer plays important roles in transportation phenomena, as pointed out by Ogasawara and Yasuda (2004), it is necessary to produce the current velocity field of the bursting layer and to develop its model, even if virtually.

This study subsumes that the influences of turbulence distributed from the wave crest to the wave trough are wholly reflected in the turbulence structure of the bursting layer. The layer's current, of which the horizontal velocity obeys the power law, is generated primarily by breaker stress. To propose a computational method of the horizontal mean velocity in the bursting layer, modeling of the Reynolds stress in the bursting layer is performed by substituting the mean flow velocity in the layer into the Reynolds equation as given values and then solving it as a reverse problem. Therefore, the modeling in this study is distinguished as a macroscopic approach based on the information of the vertical distribution of the horizontal mean velocity; it differs from the microscopic approach described above, which is based on information of the Reynolds stress. The primary purpose of this study is to propose the method described above.

An experiment using a double-bottom wind-wave tank is performed to obtain information related to the total mass flux and vertical distribution of the mean flow velocity below the wave trough and then model the Reynolds stress based on that information. Based on this result, the vertical distribution of the mean flow velocity leading to MWL is determined to make its vertical integration agree with the total mass flux. Then, the vertical distribution of the Reynolds stress is derived by solving the Reynolds equation, thereby producing a solution that agrees with the given velocity. Furthermore, the velocity of the strong wind-driven currents is separated into the mean velocity component, the shear flow turbulence, the component of the wave motion, and the breaker-induced turbulence. Furthermore, although the former turbulent flow compo-

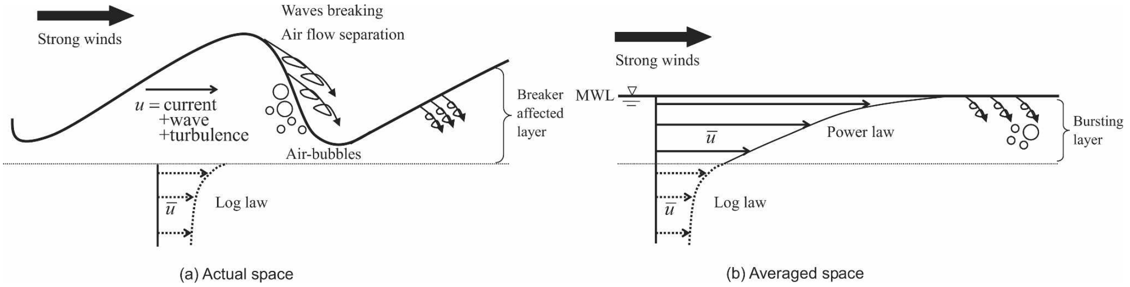

FIG. 1. Treatment of the strong wind-driven currents in (a) actual space and (b) averaged space.

nents generated by the mean shear flow are described on the basis of the Boussinesq eddy viscosity assumption, the latter turbulent flow components originated from breaking and nonbreaking waves are modeled as a breaker stress term. Finally, an averaged breaker stress term is introduced into numerical computations using a staggered mesh. Validity of the model is verified by performing a comparison of the vertical distribution of the mean flow velocity between the experimental results obtained in the double-bottom wind-wave tank and the computed results using the SOLA method (Hirt et al. 1975).

2. Bursting layer and the modeling concept

A sea surface affected by strong winds becomes covered with developed wind-wave breakers. Consequently, a surface layer with strong turbulence and surface water transport is generated (Ogasawara and Yasuda 2004). Therefore, for modeling strong wind-driven currents, it is necessary to describe the velocity and Reynolds stress in this layer correctly.

It is necessary to obtain measured data of the velocity in the surface layer to meet that information demand. However, when large and intensive water surface displacements are caused by the developed wind waves, continuous measurements of the velocity in the Eulerian coordinate become impossible because of the increased separation between the actual sea surface and MWL, which is treated as the virtual sea surface in the calculation of wind-driven currents. This obstacle is the primary difficulty that hinders modeling of the wind-driven currents affected by strong winds; the problem differs greatly from the difficulty of measurement because of the strong turbulence and air bubbles induced by wave breaking. Of course, if the required modeling is for currents driven by moderate speed wind, such essential difficulties do not arise because such a surface layer is not generated and the void region between MWL and WTL is negligible. The difficulty originates from the procedure that treats the velocity field, shown in Fig. 1a, affected by the developed wind waves, on the assumption of the averaged sea surface that the sea surface is identical to the mean sea level and that the velocity field is also identical with the mean flow field shown in Fig. 1b. Here the space shown in Fig. 1a is called the actual space, meaning that the actual ocean is treated as it is. The space shown in Fig. 1b is called the averaged space, meaning that not the actual ocean, but an averaged one, is treated for the purpose of the wind-driven current calculations.

In the actual space, the breaker-affected layer (BAL) extends from the wave crest to the interface of the power-law layer and the logarithmic law layer. The water particle velocities in the layer are influenced strongly by breaker action. On the other hand, in the averaged space, BAL is converted into the averaged breaker-affected layer (ABAL) based on the assumption of the averaged sea surface. This ABAL naturally includes all influences of wave breaking, airflow separation, and air bubbles. It can therefore be inferred that ABAL represents the macroscopic action of the breaking waves in modeling strong wind-driven currents. In addition, Ogasawara and Yasuda (2004) showed that the horizontal velocity in ABAL obeys the power law. Therefore, ABAL extends from MWL to the interface of the power-law layer and the logarithmic-law layer. It is defined as the bursting layer in the averaged space. The bursting layer is modeled to facilitate correct calculation of the horizontal velocity obeying the power law.

It is necessary to determine the vertical distribution up to MWL of the mean velocity $\overline{u}$ in the averaged space to perform modeling. Ogasawara and Yasuda (2004) showed that the value of the total mass flux q_A can be determined using the double-bottom wind-wave tank. If the value of q_A is known, then the value of the horizontal velocity $\overline{u}$ in the bursting layer can be determined to satisfy the following equation:

$$q_A = \int_{-h}^{0} \overline{u}\, dz. \qquad (1)$$

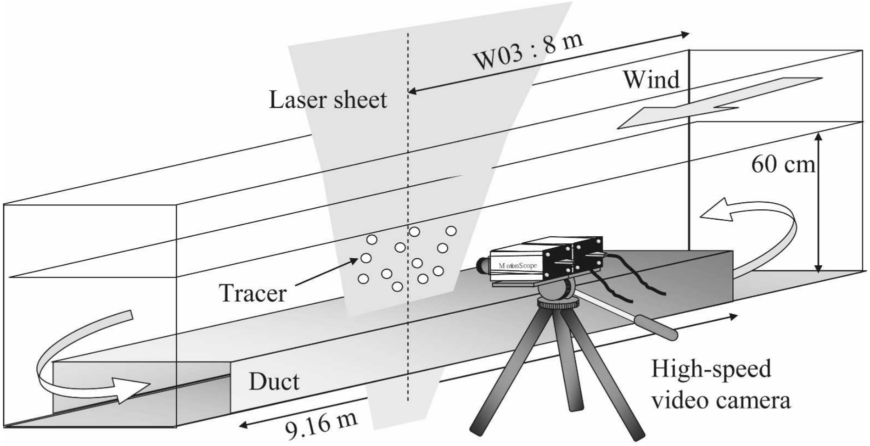

FIG. 2. Wind-wave tank with a double bottom.

Here h is defined as the distance from MWL to the upper bottom in the wind-wave tank with a double bottom. The solution of the Reynolds equation in the bursting layer must agree with the value of $\overline{u}$. The Reynolds stress term in the equation must generate the mean flow that has velocity that agrees with the value. Based on these considerations, the formulation of the breaker stress term that is the principal cause of the bursting layer is performed by substituting the vertical distribution up to MWL of $\overline{u}$ into the solution of the Reynolds equation in the bursting layer and then solving it as an inverse problem. The Reynolds equation, along with the breaker stress term formulated by the aforementioned method and the k–ε turbulence model in the bursting layer, is consequently designated as the bursting-layer model.

3. Experiments

Laboratory experiments were performed using a 15.4-m-long, 0.4-m-wide, and 1.0-m-deep double-bottom wind-wave tank, as illustrated in Fig. 2. The tank partially fulfills the continuity of the mass flux and reduces the influence of the return flow on wind-driven currents. The space between the upper and lower bottoms of the tank functions as a duct to circulate a return flow, enabling measurement of the return-flow velocity, which is disturbed only by the reverse pressure gradient within the tank. Therefore, the true wind-driven current, resulting solely from wind stress, is measurable according to the velocity of this measured return flow (Ogasawara and Yasuda 2004).

The still-water depth was fixed as 60 cm. Reference wind speeds U_r at the wind tunnel entrance were set as 6.7 m s^{-1}, yielding nonbreaking waves; 10.4 m s^{-1}, yielding partially breaking waves; and 12.0 m s^{-1}, yielding fully breaking waves. Table 1 shows values of the wave parameters governed by each wind speed at measuring point W03. Here H_s is the significant wave height, T_s the significant wave period, and f_p the peak frequency of the wave spectrum. The friction wind velocity u_{*a} was calculated using the empirical equation proposed by Wu (1980). This empirical equation tends to underestimate the value of u_{*a} compared to the measurement data derived by a regression formula based on the logarithmic law, as pointed out by Donelan (1990). This fact concurs with the experimental results obtained by Ogasawara and Yasuda (2004) in a study that used the same wind-wave tank used here. However, the difference between the values of u_{*a} calculated by the empirical equation and the measured ones is thought to be within a permissible range. Hence, instead of the values of u_{*a} based on the experimental results, the values of u_{*a} calculated through the empirical equation of Wu (1980) are to be used for winds of various speeds. Water particle velocity fields were visualized using 50-μm-diameter nylon particles and a relative density of 1.02 as tracers. Nylon particles were irradiated from the tank floor with a 5-mm-thick, 5-W power green light laser sheet. Images showing their positions were captured using two synchronized cameras with 480 × 480 pixel resolution at a 125 frames per second (fps) rate for a wind speed of 6.7 m s^{-1} and at a 250 fps rate for wind speeds of 10.4 and 12.0 m s^{-1}. The recording times of runs were 32.8 s for the wind speed of 6.7 m s^{-1}, and 16.4 s for wind speeds of 10.4

TABLE 1. Wave parameters at measurment location W03.

U_r (m s^{-1})	u_{*a} (m s^{-1})	H_s (cm)	T_s (s)	f_p (Hz)
6.7	0.24	2.50	0.35	2.89
10.4	0.40	5.59	0.51	1.92
12.0	0.48	7.46	0.58	1.73

and 12.0 m s^{-1}. The resultant images facilitated measurement of high-speed velocity fields immediately below the WTL. Velocity fields were examined using a high-resolution PIV system (Ogasawara and Yasuda 2004), which can analyze high-speed and intensively fluctuating water particle velocities affected by breaking waves.

4. Vertical distribution of the horizontal mean velocity in the bursting layer

In a bursting layer, which is generated immediately below a sea surface affected by strong winds and breaking waves, the vertical distribution of the horizontal velocity obeys a power law because the influence of turbulence is distributed from the wave crest to the wave trough (Ogasawara and Yasuda 2004). Therefore, the vertical distribution of the horizontal velocity measured in the experiment regresses to the following power-law formulation:

$$\overline{u} = \alpha(\gamma - z)^{\beta}. \tag{2}$$

Under the influence of strong winds, a large and intense water surface elevation result from the developed wind waves. For that reason, the Eulerian description cannot measure the water particle velocity fields above the wave trough continuously. Consequently, the zone between the MWL and WTL is void of measurement. Therefore, interpolation of the horizontal velocity is required for that zone. The values of α with dimensions $L^{1-\beta}T^{-1}$, the dimensionless quantity β, and γ, which has the dimension of length, are determined to produce an integrated value of $\overline{u}$ that agrees with the experimental value of the total mass flux of the wind-driven current.

The α, β, and γ parameters are formulated as functions of wind speed U_r through regression analyses. They are expressed as

$$\alpha = -1.22 \times 10^{-4}U_r^2 + 8.91 \times 10^{-3}U_r + 1.35 \times 10^{-3}, \tag{3}$$

$$\beta = -7.93 \times 10^{-5}U_r^2 - 1.10 \times 10^{-2}U_r - 0.16, \tag{4}$$

$$\gamma = \exp(-14.54) \times U_r^{2.46}. \tag{5}$$

These merely show the relation of the numerical values because the dimensions of both sides of Eqs. (3)–(5) do not correspond. Moreover, its applicability is limited to the conditions of our laboratory experiments. Nevertheless, it is noteworthy that the use of Eq. (2) together with Eqs. (3)–(5) enables us to describe the horizontal velocity $\overline{u}$ in the bursting layer including the zone between the MWL and WTL, which has heretofore lacked measurement data.

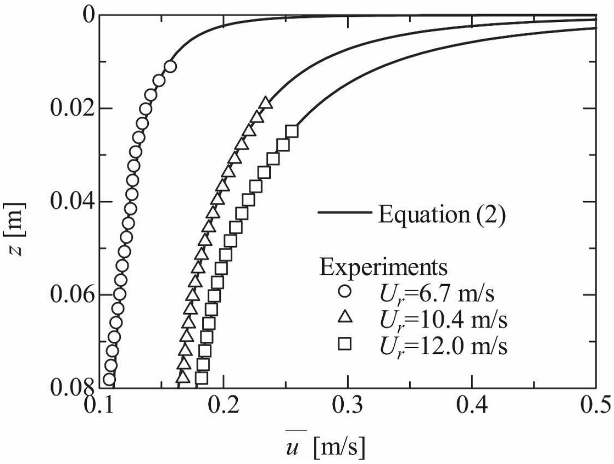

FIG. 3. Comparison of the vertical distribution of the horizontal velocity between the computed results using Eq. (2) and the measured results.

Figure 3 depicts a comparison of the vertical distribution of the horizontal velocity $\overline{u}$ between the computed results using Eq. (2) and the measured ones. Results show that Eq. (2) can describe the vertical distribution of the horizontal mean velocity in the void zone of the measurement data from the WTL to the MWL, although wind speeds merely vary from 6.7 to 12.0 m s^{-1}. In addition, the velocity distribution given by Eq. (2) in the zone below the WTL agrees well with the experimental distribution. Moreover, the velocity given by Eq. (2) increases rapidly in the region above the wave trough so that the calculated total mass flux of the wind-driven currents agrees with that of the experimental currents.

5. Division of each frequency band of velocity spectrum and its correlation

Velocity components of currents driven by strong winds comprise a mixture of the mean flow, the cascade turbulence from the mean flow (low-frequency turbulence), the wave motion, and the turbulence generated by breaking waves (high-frequency turbulence), as apparent from the shape of the velocity spectrum shown in Fig. 4. These velocity components are separable into irrotational and rotational velocity components accompanied by wave motion, turbulent flow components of which the energy source is the mean flow, and rotational wave motion, the turbulent flow components generated by wave-breaking and airflow separation, in addition to their coupled components. However, this study uses a macroscopic approach that substitutes the measurement data of the mean velocity $\overline{u}$ of the wind-driven current comprising these various velocity components into the Reynolds equation in the bursting

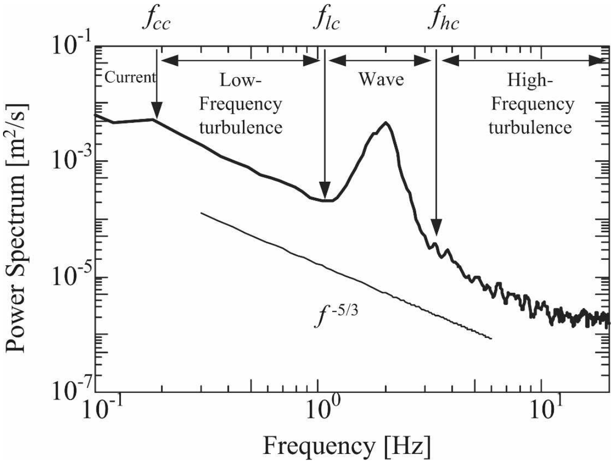

FIG. 4. Division of frequency bands of the velocity spectrum (mean flow velocity, low-frequency turbulence, wave motion, and high-frequency turbulence).

layer, solving it as a reverse problem and producing the mathematical formulation of the breaker stress, as described in section 2. Therefore, it is unnecessary to separate the velocity component of the wave motion into rotational, irrotational, turbulent flow components, and so on, as done by Thais and Magnaudet (1995) and Magnaudet and Thais (1995). Thereby, three cutoff frequencies are provided from the shape of the velocity spectrum shown in Fig. 4: f_{cc}, between the spectral band of the mean flow and the low-frequency turbulence; f_{lc}, between the low-frequency turbulence and the wave motion; and f_{hc}, between the wave motion and high-frequency turbulence. Based the cutoff frequencies, the spectral band is separable into four domains. The velocities $\mathbf{u}$ of currents driven by strong winds are treated as the sum of the mean flow velocity $\mathbf{u}_c$, the cascade turbulence velocity $\mathbf{u}_l$, the wave motion velocity $\mathbf{u}_w$, and the velocity of the breaker-generated turbulence $\mathbf{u}_h$. They are represented as

$$\mathbf{u} = \mathbf{u}_c + \mathbf{u}_l + \mathbf{u}_w + \mathbf{u}_h. \tag{6}$$

Here the velocity $\mathbf{u}_w$ of the wave motion comprises the cascading component of the shear flow turbulence and the rotational component of the wave motion. The velocity $\mathbf{u}_h$ of the breaker turbulence includes all turbulence generated by wave breaking, airflow separation, and air bubbles.

The mutual correlation among components must be known when the Reynolds average rule is applied to these components. The reverse Fourier transform is then performed to investigate the values of the correlation coefficients between respective velocity components. Table 2 shows values of the correlation tensor among horizontal and vertical velocity components at depths of $z = -3, -6, -10$ cm for respective frequency bands at the wind speed of 12.0 m s^{-1}. Results show that the value of the cross-correlation between the velocity components in different frequency bands is of negligible order at each water depth. Similar results were obtained for wind speeds of 6.7–10.4 m s^{-1}, not shown here. Even for breaker-affected velocity fields comprising a mixture of various turbulent flow components with different origins, only components in the same frequency band of the correlation tensor have nonnegligible values. For this reason, the following Reynolds average rule becomes applicable:

$$\overline{u} = u_c, \tag{7}$$

$$\overline{u_l},\ \overline{u_w},\ \overline{u_h} = 0, \tag{8}$$

$$\overline{u_c u_l},\quad \overline{u_c u_w},\quad \overline{u_c u_h} = 0, \tag{9}$$

$$\overline{u_l u_w},\quad \overline{u_l u_h} = 0, \tag{10}$$

$$\overline{u_w u_h} = 0, \tag{11}$$

$$\overline{u^2} = \overline{u_c^2} + \overline{u_l^2} + \overline{u_w^2} + \overline{u_h^2}. \tag{12}$$

In addition, the following averaging rule is applicable to the cross-correlation term $\overline{uw}$, as shown in Table 2:

$$\overline{uw} = \overline{u_c w_c} + \overline{u_l w_l} + \overline{u_w w_w} + \overline{u_h w_h}. \tag{13}$$

These are important for simplifying the treatment of the turbulence model for wind-driven currents consisting of turbulence with different origins.

6. Bursting-layer model

The mathematical formulation of the breaker stress that causes the bursting layer is performed according to the procedure explained in section 2. The Reynolds equation, which describes the horizontal velocity obeying the power law in the bursting layer, is first derived. As described in section 5, turbulent flow components with different origins exist together in the bursting layer. They are divided, as indicated in Eq. (6), and are substituted into the Navier–Stokes equation. By applying the Reynolds average rule of Eqs. (7)–(13) to it, the Reynolds equation in the x direction is derived as follows:

$$\begin{aligned}\frac{D\overline{u}}{Dt} &= -\frac{1}{\rho}\frac{\partial\overline{p}}{\partial x} + \nu\nabla^2\overline{u} - \left(\frac{\partial\overline{u_l u_l}}{\partial x} + \frac{\partial\overline{u_l v_l}}{\partial y} + \frac{\partial\overline{u_l w_l}}{\partial z}\right)\\ &\quad - \left(\frac{\partial\overline{u_w u_w}}{\partial x} + \frac{\partial\overline{u_w v_w}}{\partial y} + \frac{\partial\overline{u_w w_w}}{\partial z}\right)\\ &\quad - \left(\frac{\partial\overline{u_h u_h}}{\partial x} + \frac{\partial\overline{u_h v_h}}{\partial y} + \frac{\partial\overline{u_h w_h}}{\partial z}\right).\end{aligned} \tag{14}$$

TABLE 2. Values of correlation tensors among the horizontal and vertical velocity components at depths of $z = -3, -6, -10$ cm in each frequency band at wind speed of 12.0 m s^{-1}.

z	$\overline{u_c^2}$	$\overline{u_c u_l}$	$\overline{u_c u_w}$	$\overline{u_c u_h}$	$\overline{u_c w_l}$	$\overline{u_c w_w}$	$\overline{u_c w_h}$
-3	7.59×10^{-3}	1.50×10^{-19}	3.34×10^{-20}	1.39×10^{-21}	-1.70×10^{-20}	1.64×10^{-20}	-6.26×10^{-22}
-6	2.18×10^{-3}	7.88×10^{-20}	3.06×10^{-20}	-3.78×10^{-21}	-1.77×10^{-19}	1.30×10^{-20}	6.41×10^{-21}
-10	2.23×10^{-3}	-3.38×10^{-20}	-9.50×10^{-21}	2.19×10^{-21}	3.82×10^{-20}	-1.05×10^{-20}	1.12×10^{-21}
	$\overline{u_l^2}$	$\overline{u_l w_l}$	$\overline{u_l u_w}$	$\overline{u_l u_h}$	$\overline{u_l w_w}$	$\overline{u_l w_h}$	
-3	1.60×10^{-3}	-4.27×10^{-4}	-3.32×10^{-21}	4.51×10^{-21}	-2.09×10^{-20}	-2.52×10^{-21}	
-6	1.23×10^{-3}	-3.59×10^{-4}	-9.38×10^{-21}	-3.31×10^{-21}	-1.53×10^{-21}	-2.47×10^{-21}	
-10	7.06×10^{-4}	-7.64×10^{-5}	-2.15×10^{-20}	5.59×10^{-22}	9.87×10^{-21}	5.58×10^{-22}	
	$\overline{u_w^2}$	$\overline{u_w w_w}$	$\overline{u_w u_h}$	$\overline{u_w w_l}$	$\overline{u_w w_h}$		
-3	8.15×10^{-3}	4.03×10^{-4}	1.10×10^{-20}	-1.23×10^{-20}	-8.79×10^{-22}		
-6	6.68×10^{-3}	2.47×10^{-4}	-1.00×10^{-21}	-1.10×10^{-20}	1.38×10^{-21}		
-10	3.29×10^{-3}	9.75×10^{-5}	6.40×10^{-21}	-2.08×10^{-20}	-6.34×10^{-21}		
	$\overline{u_h^2}$	$\overline{u_h w_h}$	$\overline{u_h w_l}$	$\overline{u_l w_w}$			
-3	9.37×10^{-4}	-1.17×10^{-4}	1.78×10^{-21}	-3.18×10^{-22}			
-6	2.25×10^{-4}	-1.14×10^{-5}	4.49×10^{-21}	-1.16×10^{-20}			
-10	8.34×10^{-5}	-4.26×10^{-6}	-2.14×10^{-21}	5.72×10^{-22}			

Because the orthogonal relation holds between u_w and w_w of the irrotational wave, their inner product $-\overline{u_w w_w}$ becomes 0. However, the actual value of the inner product is not negligible; rather, it is significant because $-\overline{u_w w_w}$ comprises the turbulence generated by wave breaking, the cascading turbulence from shear mean flow, and rotational wave motion. Their primary energy source is presumed to be waves and breakers generated by strong winds in addition to that of $-\overline{u_h w_h}$. Therefore, $-\overline{u_w w_w}$ and $-\overline{u_h w_h}$ are superposed and treated collectively as the Reynolds stress $-\overline{u_t w_t}$ caused by wave and higher-frequency turbulence and are represented as

$$-\overline{u_t w_t} = -\overline{u_w w_w} - \overline{u_h w_h}. \tag{15}$$

Because $-\overline{u_t w_t}$ includes all of the turbulent flow components generated by wave motion and breakers, it is called the extended breaker turbulence. Moreover, the bursting layer is very thin. Its thickness corresponds to the significant wave height (Ogasawara and Yasuda 2004), and the relation of $\partial/\partial x$, $\partial/\partial y \ll \partial/\partial z$ is formed. Consequently, Eq. (14) is simplified as the following equation:

$$\frac{D\overline{u}}{Dt} = -\frac{1}{\rho}\frac{\partial \overline{p}}{\partial x} + \nu \frac{\partial^2 \overline{u}}{\partial z^2} - \frac{\partial \overline{u_l w_l}}{\partial z} - \frac{\partial \overline{u_t w_t}}{\partial z}. \tag{16}$$

The third term on the right-hand side is the Reynolds stress term, which originates from the mean flow. It is described by the Boussinesq eddy viscosity assumption. For instance, $-\overline{u_l w_l}$ is represented as

$$-\overline{u_l w_l} = \nu_t \frac{\partial \overline{u}}{\partial z}. \tag{17}$$

The fourth term in the rhs is the high-frequency Reynolds stress term, which originates primarily from breaking waves that cause the bursting layer. It is defined as the breaker stress term D_b as

$$D_b \equiv \frac{\partial(-\overline{u_t w_t})}{\partial z}. \tag{18}$$

Equation (16) yields the following equation:

$$\frac{\partial \overline{u}}{\partial t} = -\frac{1}{\rho}\frac{\partial \overline{p}}{\partial x} + \nu \frac{\partial^2 \overline{u}}{\partial z^2} + \frac{\partial}{\partial z}\left(\nu_t \frac{\partial \overline{u}}{\partial z}\right) + D_b. \tag{19}$$

This bursting-layer model can describe the horizontal velocity obeying the power law.

7. Formulation of the breaker stress term

Substitution of the value into Eq. (18) yields the formulation of the breaker stress term D_b if $-\overline{u_t w_t}$ in the bursting layer up to MWL is measurable using the experiment and if its value can be known. However, as described previously, it is impossible to know the value of $-\overline{u_t w_t}$ in the zone between MWL and WTL. For that reason, the following breaker stress term D_b is formulated: We substitute Eq. (2) as the solution of the Reynolds equation in the bursting layer in Eq. (19). We then solve Eq. (19) as an inverse problem for the same conditions as those of the experiment, where the currents are steady and the horizontal derivative $\partial/\partial x$ is much less than the vertical one $\partial/\partial z$,

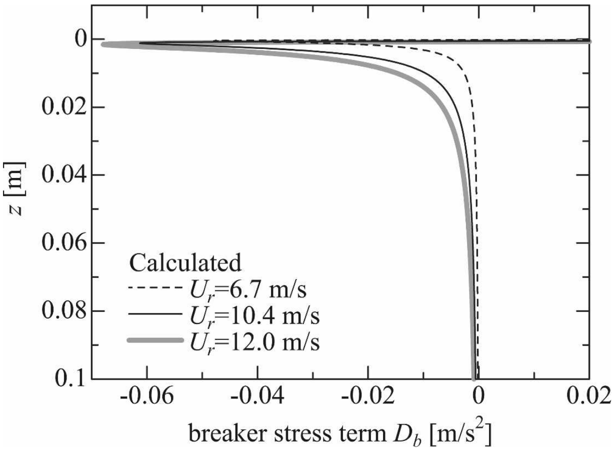

FIG. 5. Vertical distribution of the breaker stress term D_b obtained using Eq. (22).

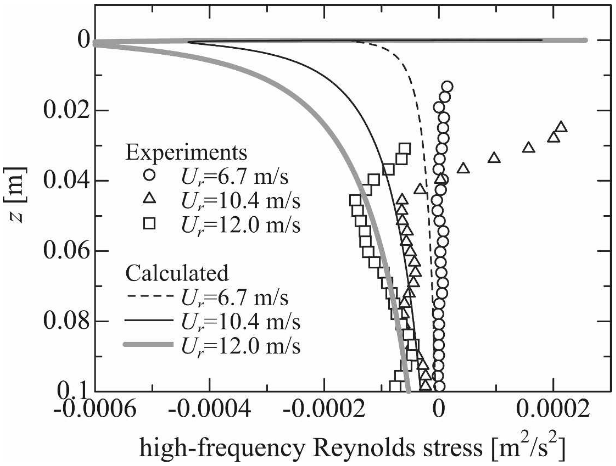

FIG. 6. Comparison of the high-frequency Reynolds stress between the value obtained from vertical integration of Eq. (22) and the experimental value.

$$D_b = -\frac{\partial}{\partial z}[-\nu_t\alpha\beta(\gamma - z)^{\beta-1}] + \psi, \qquad (20)$$

in which ψ is assumed to be of negligible order. Therefore, ψ is treated as zero, $\psi \approx 0$, henceforth. In that equation, ν_t is the eddy viscosity coefficient. The modeling of the Reynolds stress in the bursting layer is performed on the assumption of the averaged sea surface. In that case, the scale of vortices in the model is limited by the distance from the sea surface since the sea surface is treated virtually as a rigid lid at MWL. Consequently, the law of the wall holds in the layer; ν_t is represented on the basis of the mixing length theory as

$$\nu_t = \kappa u_*(-z + z_0). \qquad (21)$$

Substitution of Eq. (21) into Eq. (20) yields the breaker stress term D_b, which is represented as

$$D_b = -\kappa u_*\alpha\beta(\gamma - z)^{\beta-1}[1 + (-z + z_0)(\beta - 1)(\gamma - z)^{-1}] \qquad (22)$$

in which κ represents von Kármán's constant and z_0 is the roughness length.

Figure 5 shows the vertical distribution of D_b obtained using the aforementioned procedure. Here D_b has a positive value in the zone immediately below the MWL but has a negative value in the lower zone. Therefore, the breaker stress acts as a strong driving force in the positive zone, but it acts oppositely as a resistance in the negative zone. Moreover, the vertical distribution of D_b becomes steeper with increased wind speed.

As shown by Eq. (18), the vertical integration of D_b yields the high-frequency Reynolds stress $-\overline{u_t w_t}$. Its value, obtained from the vertical integration of Eq. (22), is compared with the experimental one. That result is shown in Fig. 6. At the wind speed of 6.7 m s^{-1}, the water surface is in a state of ripples and is regarded as nonbreaking in the normal water wave scale, that is, microbreaking waves. Consequently, the experimental value of the high-frequency Reynolds stress is almost uniformly 0 along the vertical axis. The calculated value agrees well with the experimental one, but it has its minimum value point immediately below the water surface. Experimental values for wind speeds of 10.4 and 12.0 m s^{-1} are those for breaking waves; they have a minimum value at a location approximately 0.04 m deep from MWL. The values increase rapidly toward MWL from that location. The distribution of the calculated value agrees well with that of the experimental one over the domain from the bottom to the minimum value point. However, above the minimum value point, the difference between the calculated values and the experimental ones increases remarkably.

Although this difference is partially attributable to the approximation $\psi \approx 0$, it is more directly attributable to the following treatment: The experimental value is based on the measurement of the actual velocity fields that are directly affected by the water surface displacement, whereas the calculated value is obtained based on the assumption of the averaged sea surface. The calculated value is obtained by assuming that the bursting layer is immediately below the averaged sea surface, and then by averaging the turbulent flow components not only in the horizontal direction but also in the vertical direction. Different methods are used to obtain the calculated values and the experimental ones. For that reason, it is natural that the values do not concur. When a numerical computation is performed for the

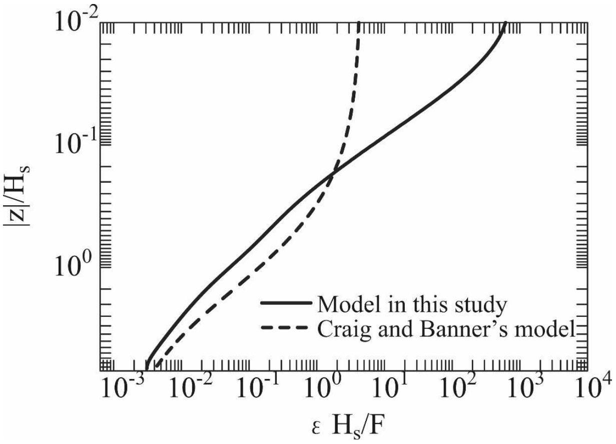

FIG. 7. Vertical distribution of the normalized dissipation rate, $\varepsilon H_s/F$, obtained using the present method and Craig and Banner (1994) model: $F = 100u_*^3$ is the flux of the kinetic energy from wind to waves.

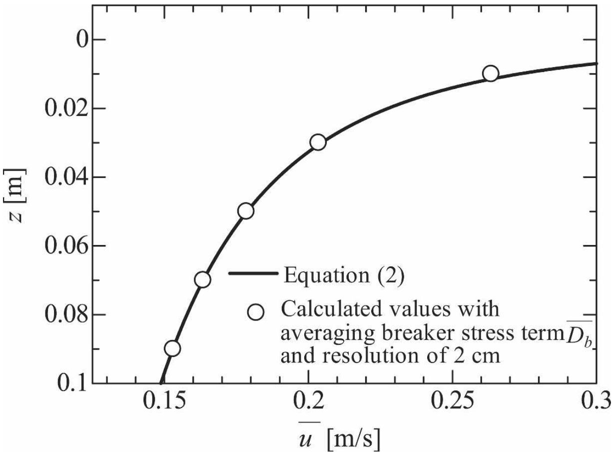

FIG. 8. Comparison of the horizontal velocity between the computed value using $\overline{D_b}$ and the analytical solution of Eq. (24) at a wind speed of 10.4 m s^{-1}.

wind-driven currents with developed waves generated by strong winds, it is impossible to describe the horizontal velocity obeying the power law in the bursting layer as far as the experimental values of the high-frequency Reynolds stress simply extrapolated to MWL is employed. In fact, the horizontal velocity obeying the power law can be described using the value of D_b obtained by Eq. (22) on the assumption of the averaged sea surface. This will be verified in section 8.

Figure 7 shows the vertical distribution of normalized dissipation rate $\varepsilon H_s/F$ ($F = 100u_*^3$ is the flux of the kinetic energy from wind to waves), as calculated by substituting the horizontal mean velocity $\overline{u}$ expressed by Eq. (2) into the k–ε turbulence model and solving it. Moreover, the vertical distribution of $\varepsilon H_s/F$, calculated by a model proposed by Craig and Banner (1994), is also shown in Fig. 7 for comparison. Soloviev and Lukas (2006) showed measurement data of $\varepsilon H_s/F$ in the depth below $|z|/H_s = -0.2$ in their work. The values of $\varepsilon H_s/F$ calculated in this study agree well with the measurement data and the result of Craig and Banner's model. In the zone $|z|/H_s = 0$ to -0.2, for which measurement data are nonexistent, the difference between the values of $\varepsilon H_s/F$ calculated in this study and those calculated by Craig and Banner's model increases. The modeling performed in this study is a macroscopic approach based on the assumption of an averaged sea surface, as described above. In contrast, modeling by Craig and Banner is based on a microscopic approach. It is inferred that the difference of both approaches results in that of values of ε immediately below the sea surface.

Figure 5 shows that the vertical distribution of D_b is very steep near the MWL. Its minimum value point for wind speed 10.4 m s^{-1} is located at the depth of 5×10^{-4} cm below the MWL. It is necessary to reproduce the steep distribution of D_b with the minimum value when numerical computation is performed. A vertical resolution of 5×10^{-4} cm or less is required to satisfy this request. However, this is impossible from the viewpoint of computing time. For that reason, the following averaging breaker stress term $\overline{D_b}$ is proposed for use instead of D_b:

$$\overline{D_b} = \kappa u_* \alpha\beta[(-z_2 + z_0)(\gamma - z_2)^{\beta-1} - (-z_1 + z_0)(\gamma - z_1)^{\beta-1}]/\Delta z. \tag{23}$$

This equation is obtained by integrating D_b, defined at the half level in the staggered grid from the bottom z_1 of the lattice to the top z_2, and then dividing it by grid spacing Δz.

Figure 8 shows the vertical distribution of the horizontal velocity. It is obtained by solving the following Reynolds equation in the bursting layer containing the averaging breaker stress term $\overline{D_b}$ in Eq. (23) using a finite difference method:

$$\frac{\partial \overline{u}}{\partial t} = \frac{\partial}{\partial z}\left(\nu_t \frac{\partial \overline{u}}{\partial z}\right) + \overline{D_b}. \tag{24}$$

The vertical resolution was assumed as 2 cm; the wind speed was set as 10.4 m s^{-1}. The initial condition was in the state of still water. Calculations were performed until they achieved a steady state. Moreover, because the analytical solution of Eq. (24) in the steady state is given as Eq. (2), it is also shown in Fig. 8 for comparison. Figure 8 shows that the result of numerical calculation using $\overline{D_b}$ agrees well with the analytical solution, but that the resolution is 2 cm and rough. This result demonstrates the efficiency of the averaging breaker stress term.

8. Calculation reproducing experiment results

Calculations to reproduce wind-driven currents in experiments are undertaken next. Those results are then compared to measured values to verify that construction of the bursting-layer model was performed appropriately.

The fundamental equations are the following continuity equation and bursting layer Reynolds equations in the vertical two-dimensional domain:

$$\frac{\partial \overline{u}_j}{\partial x_j} = 0, \tag{25}$$

$$\frac{\partial \overline{u}_i}{\partial t} + \overline{u}_j \frac{\partial \overline{u}_i}{\partial x_j} = -\frac{1}{\rho}\frac{\partial \overline{p}}{\partial x_i}\left(P + \frac{2}{3}k\right) + \frac{\partial}{\partial x_j}\left[(\nu + \nu_t)\left(\frac{\partial \overline{u}_i}{\partial x_j} + \frac{\partial \overline{u}_j}{\partial x_i}\right)\right] + \mathbf{g} + \overline{\mathbf{D_b}}, \tag{26}$$

where $\mathbf{g} = (0, -g)$ and $\overline{\mathbf{D_b}} = (\overline{D_b}, 0)$.

The eddy viscosity coefficient that is necessary to represent the Reynolds stress resulting from the mean shear flow in Eq. (26) is obtained by solving the following k–ε turbulence model:

$$\nu_t = C_\mu \frac{k^2}{\varepsilon}, \tag{27}$$

$$\frac{\partial k}{\partial t} + \overline{u}_j \frac{\partial k}{\partial x_j} = P_k - \varepsilon + \frac{\partial}{\partial x_j}\left[\left(\frac{\nu_t}{\sigma_k} + \nu\right)\frac{\partial k}{\partial x_j}\right], \tag{28}$$

$$\frac{\partial \varepsilon}{\partial t} + \overline{u}_j \frac{\partial \varepsilon}{\partial x_j} = (C_{\varepsilon 1}P_k + C_{\varepsilon 2}\varepsilon)\frac{\varepsilon}{k} + \frac{\partial}{\partial x_j}\left[\left(\frac{\nu_t}{\sigma_\varepsilon} + \nu\right)\frac{\partial \varepsilon}{\partial x_j}\right]. \tag{29}$$

In those equations, P_k is the shear production term and is defined as

$$P_k = \frac{\nu_t}{2}\left(\frac{\partial \overline{u}_i}{\partial x_j} + \frac{\partial \overline{u}_j}{\partial x_i}\right)\left(\frac{\partial \overline{u}_i}{\partial x_j} + \frac{\partial \overline{u}_j}{\partial x_i}\right). \tag{30}$$

Moreover, standard values $C_\mu = 0.09$, $\sigma_k = 1.0$, $\sigma_\varepsilon = 1.3$, $C_{\varepsilon 1} = 1.44$, and $C_{\varepsilon 2} = 1.92$ are used as experimental constants. However, the values of σ_ε and others are experimental constants obtained on the assumption of the logarithmic law. Although it is problematic that these values are applied without modification to the bursting layer of the wind-driven currents obeying the power law, their application is a task for future study.

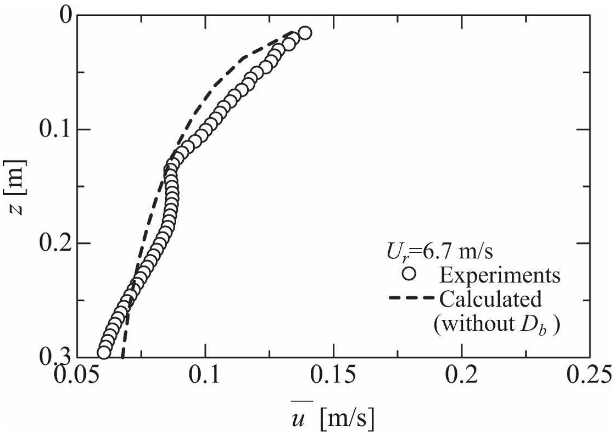

FIG. 9. Comparison of the vertical distribution of the horizontal velocity between the computational result and the experimental result at a wind speed of 6.7 m s^{-1} for a nonbreaking wave.

Discrimination of these equations is performed using a finite difference method on a staggered grid. Their solutions are obtained using the SOLA method (Hirt et al. 1975). The calculation domain is assumed to be of the same scale as that of the double-bottom wind-wave tank (Fig. 2) used in the experiment; the lower duct was installed, as in the experiment. In that calculation, the time step is set as 0.001 s, the horizontal resolution is set as 0.3 m, and the vertical resolution is set as 0.025 m. The initial state is assumed to be still water. Calculation of the wind-driven current is performed until it approaches the steady state. Calculated values of the horizontal velocity of the current are compared with the experimental ones at the same location W03 with those derived through the experiment.

Figure 9 presents a comparison of the vertical distribution of the horizontal velocity between the computational result and the experimental one for wind speed of 6.7 m s^{-1}, which is in the regime of nonbreaking waves. For that reason, the breaker stress term is not used. The present model well describes the experimental result. It is verified that the calculation performed using the aforementioned method can appropriately calculate the wind-driven currents in the regime of nonbreaking waves. In addition, this method can calculate the wind-driven currents in the regime of breaking waves, but only if breaker stress modeling is performed appropriately.

Figure 10 presents a comparison of the vertical distribution of the horizontal velocity between the computational and experimental results for a wind speed of 10.4 m s^{-1}. Here, the computational result using the breaker stress term (with D_b) and the computational result not using the breaker stress term (without D_b) are shown for comparison. The conventional calculation, without D_b, is incapable of describing the steep

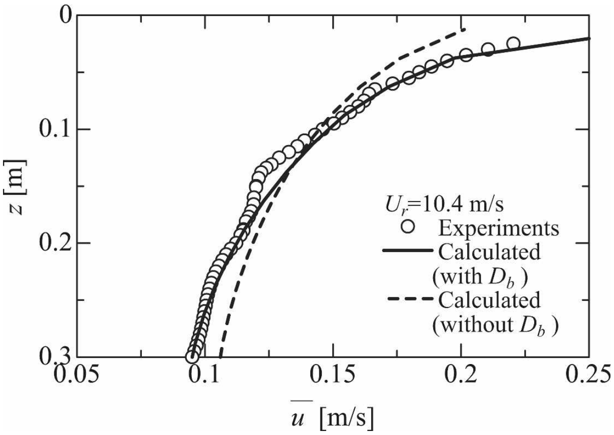

FIG. 10. Comparison of the vertical distribution of the horizontal velocity between the computational result and the experimental result at a wind speed of 10.4 m s^{-1} for a breaking wave.

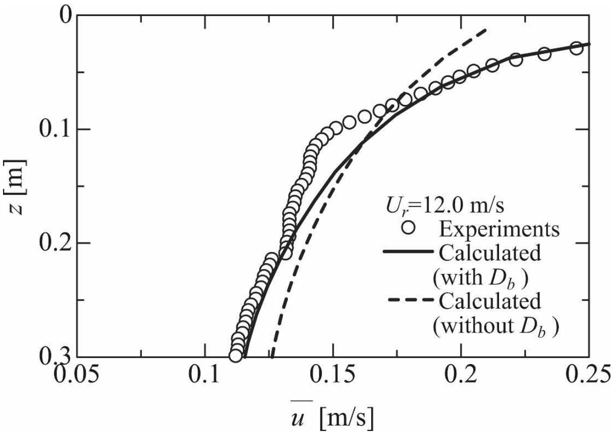

FIG. 11. As in Fig. 10, but at a wind speed of 12.0 m s^{-1}.

vertical distribution in the bursting layer, with thickness of approximately 5.5 cm affected by strong winds. The conventional calculation is also incapable of describing the distribution in the layer that is lower than the bursting layer. The distribution is underestimated (overestimated) in the upper (lower) layer. In contrast, the calculation with D_b can appropriately describe not only the steep vertical distribution in the bursting layer, but it can also describe the distribution in the lower layer. This capability arises from characteristics of the Reynolds stress generated by the breaking waves, which act as an extremely strong driving force immediately below the MWL. They act oppositely, resistant to the lower layer, as described above.

Figure 11 presents a comparison of the vertical distribution of the horizontal velocity between the computational and the experimental results at the wind speed 12.0 m s^{-1}. As shown in that figure, the conventional calculation without D_b cannot describe the steep vertical distribution obeying the power law in the bursting layer, of which thickness is approximately 7.5 cm. Moreover, it is overestimated in the lower layer. The accuracy of calculation of velocity with steep vertical distribution obeying the power law is improved using D_b.

Results show that modeling that includes the breaker stress term is appropriate.

9. Conclusions

This paper presented a method for formulating an extended breaker stress term. Using that term, we can correctly describe the vertical distribution up to MWL of the horizontal velocity of strong wind-driven currents. It uses a macroscopic approach, treating the overall breaker action based on the assumption of the averaged sea surface. The primary results obtained in this study are summarized as follows:

- The velocity of the strong wind-driven currents in the region between WTL and a virtual sea surface (MWL) lacking measurements was extrapolated to make their vertical integration agree with the total mass flux measured in the experiment, based on experimental results obtained using a double-bottom wind-wave tank and a high-resolution PIV system.
- The bursting layer is defined as a turbulent boundary layer that is affected by various actions, such as wave breaking, airflow separation, and air bubbles, by a macroscopic approach to the assumption of the averaged sea surface. Thickness of the bursting layer extends from MWL to the interface of the power-law layer and the logarithmic law layer.
- Experimental results demonstrate that the Reynolds stress is separable into a low-frequency component that originates from the mean shear flow and a high-frequency component that originates from wind-wave breakers. The high-frequency component that causes the bursting layer is newly defined as the breaker stress.
- The vertical distribution of the extended breaker stress was formulated by substituting the values of the mean flow velocity $\overline{u}$ into the Navier–Stokes equation and solving it as a reverse problem.
- The vertical distributions of $-\overline{u_t w_t}$ and ε in the bursting layer, including the void zone of measurements, were shown using information on the vertical distribution of the mean flow velocity $\overline{u}$.
- The Reynolds equation, including the breaker stress term and the k–ε turbulence model, were derived as governing equations of the bursting layer. They were treated as the bursting-layer model.

- Numerical computations using the bursting-layer model were performed to reproduce strong wind-driven currents in the double-bottom wind-wave tank. Results verified that the bursting-layer model accurately calculated the steep vertical distribution of the current velocity in the bursting layer.

Acknowledgments. This research work was supported by a Grant-in-Aid for Scientific Research 18360236 from the Japan Society for the Promotion of Science.

REFERENCES

Banner, M. L., and W. L. Peirson, 1998: Tangential stress beneath wind-driven air–water interfaces. *J. Fluid Mech.,* **364,** 115–145.

Cheung, T. K., and R. L. Street, 1988a: The turbulent layer in the water at an air-water interface. *J. Fluid Mech.,* **194,** 133–151.

——, and ——, 1988b: Wave-following measurements in the water beneath an air-water interface. *J. Geophys. Res.,* **93,** 14 089–14 097.

Craig, P. D., 1996: Velocity profiles and surface roughness under breaking waves. *J. Geophys. Res.,* **101,** 1265–1278.

——, and M. L. Banner, 1994: Modeling wave-enhanced turbulence in the ocean surface layer. *J. Phys. Oceanogr.,* **24,** 2546–2559.

Donelan, M. A., 1990: Air-sea interaction. *The Sea,* B. LeMehaute and D. M. Hanes, Eds., Ocean Engineering Science, Vol. 9, Wiley and Sons, 239–292.

Gargett, A. E., 1989: Ocean turbulence. *Annu. Rev. Fluid Mech.,* **21,** 419–451.

Hirt, C. W., B. D. Nichols, and N. C. Romero, 1975: SOLA: A numerical solution algorithm for transient fluid flows. Los Alamos Scientific Laboratory Tech. Rep. LA-5852, 50 pp.

Kitaigorodskii, S. A., M. A. Donelan, J. L. Lumley, and E. A. Terray, 1983: Wave–turbulence interactions in the upper ocean. Part II: Statistical characteristics of wave and turbulent components of the random velocity field in the marine surface layer. *J. Phys. Oceanogr.,* **13,** 1988–1999.

Lin, J. T., and M. Gad-el-Hak, 1984: Turbulent current measurements in a wind-wave tank. *J. Geophys. Res.,* **89,** 627–636.

Magnaudet, J., and L. Thais, 1995: Orbital rotational motion and turbulence below laboratory wind water waves. *J. Geophys. Res.,* **100,** 757–772.

Mellor, G., and A. Blumberg, 2004: Wave breaking and ocean surface layer thermal response. *J. Phys. Oceanogr.,* **34,** 693–698.

Ogasawara, T., and T. Yasuda, 2004: Mass flux and vertical distribution of currents caused by strong winds in a wave tank. *J. Phys. Oceanogr.,* **34,** 2712–2720.

Soloviev, A., and R. Lukas, 2006: Near-surface turbulence. *The Near-Surface Layer of the Ocean: Structure, Dynamics and Applications,* Springer, 144–217.

Thais, L., and J. Magnaudet, 1995: A triple decomposition of the fluctuating motion below laboratory windwater waves. *J. Geophys. Res.,* **100,** 741–756.

Thorpe, S. A., 1992: Bubble clouds and the dynamics of the upper ocean. *Quart. J. Roy. Meteor. Soc.,* **118,** 1–22.

Wu, J., 1980: Wind-stress coefficients over sea surface near neutral conditions—A revisit. *J. Phys. Oceanogr.,* **10,** 727–740.

Zhang, X. J., and C. S. Cox, 1999: Vortical motions under short wind waves. *Wind-Driven Air-Sea Interface: Air–Sea Interface Symp.,* Sydney, Australia, The University of New South Wales, 277–284.